S- and p-wave structure of $S = -1$ meson-baryon scattering in the resonance region

D. Sadasivan,[1,*] M. Mai,[1,†] and M. Döring[1,2,‡]

[1] *Institute for Nuclear Studies and Department of Physics, The George Washington University, Washington, DC 20052, USA*

[2] *Thomas Jefferson National Accelerator Facility, Newport News, VA 23606, USA*

We perform a simultaneous analysis of s- and p-waves of the $S = -1$ meson-baryon scattering amplitude using all low-energy experimental data. For the first time, differential cross section data are included for chiral unitary coupled-channel models. From this model s- and p-wave amplitudes are extracted and both well-known $I(J^P) = 0(1/2^-)$ s-wave states as well as a new state in the p-wave are observed. While the latter passed multiple statistical and phenomenological robustness tests, its existence is at odds with Quark Model predictions and recent Lattice results. Possible explanations are discussed in this work.

PACS numbers: 11.30.Rd, 11.80.Gw, 14.20.Jn

Introduction Strangeness plays an important role in various facets of strongly interacting matter. For example, the attractive interaction between antikaons and nucleons leads to the famous $\Lambda(1405)$-resonance as predicted in Ref. [1]. Nowaday this low-energy $S = -1$ energy region is accessed by chiral unitary coupled-channel models [2–19], amplitude analyses [20–25], lattice QCD [26–30], and quark models [31–33], see, e.g., the reviews in Refs. [34, 35]. A similar mechanism can be responsible for the generation of K^-pp bound states, being searched for by, e.g., FINUDA [36]. Furthermore, the equation of state of neutron stars is sensitive to the antikaon condensate [37, 38] and thus to the propagation of antikaons in nuclear medium. In the era of high-precision measurements of neutron star properties with LIGO [39], this ultimately can lead to new interconnection between QCD and astrophysical observations.

At the core of all theoretical studies lies the antikaon-nucleon scattering amplitude, which has to address the non-perturbative regime of QCD valid over a large energy range including the resonance region. Such a "twice non-perturbative" amplitude can neither rely on perturbative QCD nor its low-energy effective field theory. Thus, some model dependence has to be introduced, with the corresponding parameters being fitted to experimental data. In this work we use the model derived in a series of works [2, 40] which to our knowledge is the only approach, which has the correct low-energy behavior, fulfills two-body unitarity and describes s- and p-waves simultaneously. This property is utilized to fit all available scattering and threshold data including (for the first time) differential cross sections, simultaneously, up to energies well below the d-wave $\Lambda(1520)3/2^-$ resonance.

Model The entire database for meson-baryon scattering in the strangeness $S = -1$ sector comes from experiments with K^-p in the initial state. In general, 10 combinations of ground state octet mesons and baryons have the same quantum numbers, i.e. $\mathcal{S} := \{K^-p, \bar{K}^0n, \pi^0\Lambda, \pi^0\Sigma^0, \pi^+\Sigma^-, \pi^-\Sigma^+, \eta\Lambda, \eta\Sigma^0, K^+\Xi^-, K^0\Xi^0\}$ meaning that the scattering amplitude T must describe the dynamics of all coupled-channels simultaneously. Two-body unitarity constrains the form of such a scattering amplitude, being incorporated exactly via the Bethe-Salpeter equation in d Minkowski dimensions

$$T(\not{q}_2, \not{q}_1; p) = V(\not{q}_2, \not{q}_1; p) + i \int \frac{d^d\ell}{(2\pi)^d} \frac{V(\not{q}_2, \not{\ell}; p)}{\ell^2 - M^2 + i\epsilon} \frac{1}{\not{p} - \not{\ell} - m + i\epsilon} T(\not{\ell}, \not{q}_1; p)\,, \tag{1}$$

where p is the total and $q_{1/2}$ are the in-/outgoing meson four-momenta, and m/M denote the mass of the baryon/meson in each channel, respectively. Different channels are related by $\mathrm{SU(3)_f}$ symmetry and its breaking in the interaction kernel V and can be further restricted by demanding the correct energy-dependence around the corresponding thresholds. This requirement is addressed by taking the ChPT [41] local potential up to the next-to-leading chiral order

$$V(\not{q}_2, \not{q}_1; p) = A_{WT}(\not{q}_1 + \not{q}_2) + A_{1-4}(q_1 \cdot q_2) + A_{5-7}[\not{q}_1, \not{q}_2] + A_{0DF} + A_{8-11}\Big(\not{q}_2(q_1 \cdot p) + \not{q}_1(q_2 \cdot p)\Big)\,, \tag{2}$$

where A are matrices over the channel space that depend on the meson decay constants (fixed throughout this work together with meson and baryon masses to the physical values [35]) and low-energy constants (LECs) $\{b_0, b_D, b_F, b_1, ..., b_{11}\}$. The latter are not known from ChPT and must be fitted to the experimental data.

The present model corresponds to an infinite sub-set of all ChPT Feynman diagrams. Missing topologies yield in the fact that the regularization scale of the loop integration in Eq. (1) does not cancel. In other words, it parametrizes the missing Feynman topologies to some extent and is dealt with as free parameters of the model. Neglecting isospin breaking, there are six such parameters, called $\{a_i | i = 1, .., 6\}$ in the following for brevity. Previous analyses [3, 40, 42] have shown that off-shell terms explicitly contained in Eq. (1) have only minor effect and are dropped here as well. With this approximation the scattering amplitude is solved analytically and is

$\chi^2_{\rm dof}$	1.10 (62/30/8%)
$\lvert\Sigma\rvert$ [GeV^{-14}]	0.106

a_{1-6}	b_{1-11} [GeV^{-1}]
$+0.44^{+0.28}_{-0.14}$	$-0.34^{+0.11}_{-0.04}$
$+2.04^{+1.37}_{-0.50}$	$+0.29^{+0.21}_{-0.18}$
$+0.14^{+0.15}_{-0.20}$	$-0.62^{+0.04}_{-0.06}$
$-0.95^{+0.30}_{-0.31}$	$-0.02^{+0.16}_{-0.14}$
$-0.75^{+0.16}_{-0.45}$	$+0.24^{+0.06}_{-0.11}$
$-1.99^{+0.30}_{-3.59}$	$-0.82^{+0.31}_{-0.09}$
	$-1.32^{+0.44}_{-0.04}$
$b_{0,D,F}$ [GeV^{-1}]	$-0.01^{+0.02}_{-0.10}$
$-0.50^{+0.01}_{-0.01}$	$+0.04^{+0.22}_{-0.14}$
$+0.08^{+0.01}_{-0.01}$	$+0.15^{+0.05}_{-0.06}$
$-0.22^{+0.01}_{-0.01}$	$+0.40^{+0.13}_{-0.05}$

$I(J^P)$		$0(1/2^-)$	$0(1/2^-)$	$1(1/2^+)$
Pole position [MeV]		$1430-15i$	$1360-43i$	$1360-11i$
Covariance [MeV^2]		$\begin{pmatrix} +20.0 & +3.7 \\ & +14.9 \end{pmatrix}$	$\begin{pmatrix} +169 & -166 \\ & +202 \end{pmatrix}$	$\begin{pmatrix} +354 & -91 \\ & +31 \end{pmatrix}$
Couplings [GeV]	g_{K^-p}	$0.34^{+0.10}_{-0.05}$	$0.35^{+0.06}_{-0.03}$	$0.10^{+0.05}_{-0.03}$
	$g_{\bar{K}^0n}$	$0.32^{+0.10}_{-0.05}$	$0.35^{+0.06}_{-0.04}$	$0.10^{+0.04}_{-0.03}$
	$g_{\pi^0\Lambda}$	–	–	$0.19^{+0.03}_{-0.03}$
	$g_{\pi^0\Sigma^0}$	$0.19^{+0.03}_{-0.02}$	$0.39^{+0.04}_{-0.03}$	–
	$g_{\pi^+\Sigma^-}$	$0.19^{+0.03}_{-0.02}$	$0.40^{+0.04}_{-0.03}$	$0.11^{+0.06}_{-0.07}$
	$g_{\pi^-\Sigma^+}$	$0.19^{+0.03}_{-0.02}$	$0.38^{+0.04}_{-0.03}$	$0.09^{+0.06}_{-0.06}$
	$g_{\eta\Lambda}$	$0.22^{+0.23}_{-0.09}$	$0.30^{+0.10}_{-0.07}$	–
	$g_{\eta\Sigma^0}$	–	–	$0.13^{+0.25}_{-0.07}$
	$g_{K^+\Xi^-}$	$0.05^{+0.03}_{-0.03}$	$0.02^{+0.02}_{-0.01}$	$0.08^{+0.07}_{-0.06}$
	$g_{K^0\Xi^0}$	$0.06^{+0.03}_{-0.03}$	$0.02^{+0.02}_{-0.01}$	$0.08^{+0.07}_{-0.06}$

TABLE I: Left: Parameters of the best fit. The values in parentheses behind the χ^2dof show the contributions from data sets (a,b,c), respectively. The generalized variance is given by the determinant of the covariance matrix, $|\Sigma|$. Error bars on the model parameters are determined in a re-sampling procedure. Right: Prediction of resonance parameters found in a channel of given isospin (I) and total angular momentum ($J = L \pm 1/2$) on the second Riemann sheet, including couplings to meson-baryon channels.

projected to physical observables [43]. To our knowledge this model is the only existing unitary coupled-channel model which contains explicit s- and p-wave interactions, derived from the low-energy behavior of QCD Green's functions.

Data and fits The available data consist of: (a) Total cross sections [44–47] for $\{K^-p \to \mathcal{S}_i \,|i = 1,..,6\}$ in the lab-momentum range of $P_{lab} < 300$ MeV; (b) Differential cross sections [48] in the same momentum window for the $K^-p \to K^-p$ and $K^-p \to \bar{K}^0n$ reactions; (c) Threshold decay ratios [49, 50] $\gamma = 2.38 \pm 0.04$, $R_n = 0.189 \pm 0.015$, $R_c = 0.664 \pm 0.011$, and energy shift ($\Delta E = 283 \pm 42$ eV) and width ($\Gamma = 541 \pm 110$ eV) of kaonic hydrogen measured in the SIDDHARTA [51] experiment and related [52] to the K^-p complex-valued scattering length a_{K^-p}. Further experimental data, related indirectly to the $\bar{K}N$ scattering amplitude, require additional model assumptions and are not used in fits. *A-posteriori* checks to these data will be discussed below.

We employ a multi-step fitting routine to explore the parameter space as extensively as possible. First, we set all parameters b to zero, effectively reducing the chiral order of the driving term V of Eq. (1). The remaining parameters are fitted to the data starting from a large set $\mathcal{O}(10^3)$ of randomized starting values of natural size, i.e. $|a_i| \lesssim 5$. Second, using the best fits of the previous step as starting values we fit all parameters of the model simultaneously. The starting values of the so-called dynamical LECs $b_1 - b_{11}$ are chosen randomly and fitted within natural limits $|b_{1-11}| < 10$ GeV^{-1}. The starting values of the symmetry-breaking LECs b_0, b_D, b_F are chosen such that the next-to-leading order chiral formulae [41] yield $\sigma_{\pi N} = 45$ MeV and physical values for ground-state octet baryon masses. In the fit, small variations around these values are allowed. We found that this stabilizes the fit considerably. At every step of the fit routine, we impose an analyticity constraint on the scattering amplitude, disregarding solutions with poles on the first Riemann sheet closer than 150 MeV to the real axis.

The obtained best fit has an order of magnitude smaller $\chi^2_{\rm dof}$ than the next best fits. Its parameters are collected in the left panel of Tab. I. The experimental data is well reproduced by the model as shown in Figs. 3 and 4 in the Appendix. The major contribution to the $\chi^2_{\rm dof}$ originates from the total cross sections data (a), see values in parenthesis. All model parameters are of natural size with 1σ-uncertainties determined in a re-sampling procedure. The quantity $|\Sigma|$ shows the generalized variance that is proportional to the volume of the error ellipse of the 20-dimensional parameter space which can serve as a bulk measure of how well the data restrict the parameters. Exploring the covariance matrix, we have not found any obvious separation between various parameter groups.

The interaction kernel (2) contains explicit (linear) dependence on the (cosine of) scattering angle, and so does the solution of the dynamical coupled-channel equation (1). The best fit solution is projected to the s- and p-waves, denoted as in Ref. [43] by $f^I_{L\pm}$, indicating total angular momentum $J = L \pm 1/2$ and isospin I. This is

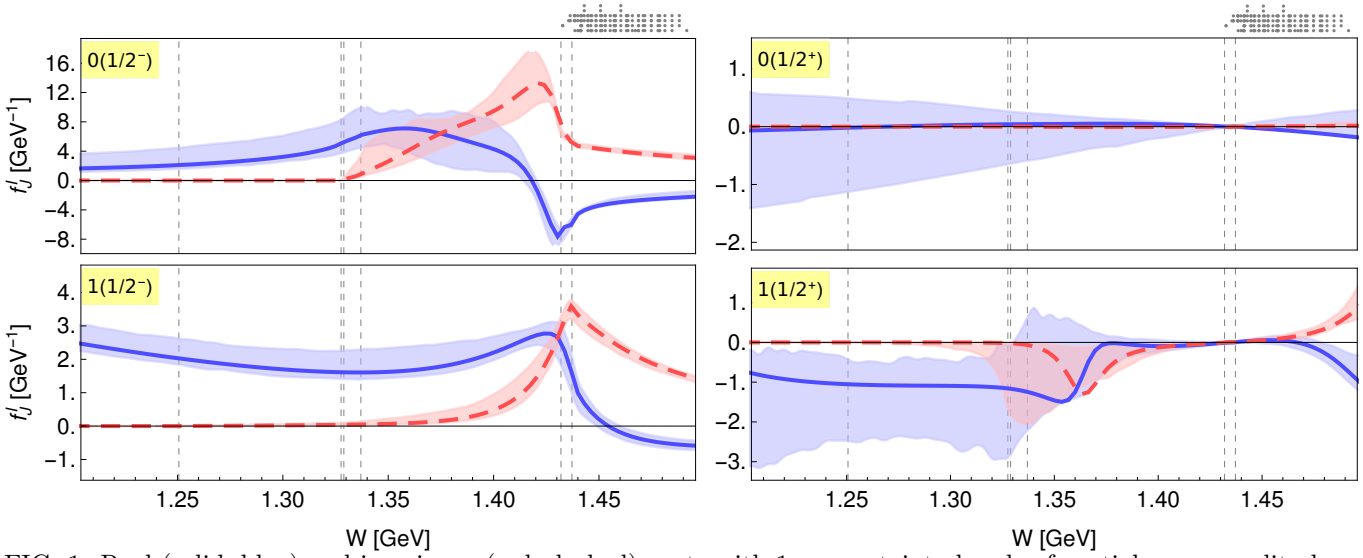

FIG. 1: Real (solid, blue) and imaginary (red, dashed) parts with 1σ uncertainty bands of partial wave amplitudes with $I(J^P)$. The vertical dashed lines show the positions of the $\pi\Lambda$, $\pi^0\Sigma^0$, $\pi^+\Sigma^-$, $\pi^-\Sigma^+$, K^-p, $\bar{K}^0n$ thresholds, and the dots over the plots represent the available data in the respective channel from top to bottom.

depicted in Fig. 1 including 1σ error bands up to energies covered by the considered data base (see dots above Fig. 1). Around the $\bar{K}N$ threshold the dominant contribution is due to the s-wave amplitudes with a clear resonant behavior in the sub-threshold region in the isoscalar channel.

To identify the resonance parameters the amplitudes $f^I_{L\pm}$ are analytically continued to the complex energy-plane on the second Riemann sheet (II.RS). Indeed, on the II.RS connected to the physical one between the $\pi\Sigma$ and $\bar{K}N$ thresholds we find two poles in the $0(1/2^-)$ sector, associated with the $\Lambda(1405)$, and one in the $1(1/2^+)$ channel, referred in the following to as $\Sigma(1380)1/2^+$.

The resonance parameters are collected in the right panel of Tab. I, including the magnitudes of the couplings to the meson-baryon channels $g^2 := |\lim_{W\to W*}(W-W^*)f^I_{L\pm}(W)|$ for the pole position W^*. As expected, the narrow pole of the $\Lambda(1405)$ couples dominantly to $\bar{K}N$, while the broad one more to the $\pi\Sigma$ channels. The new $\Sigma(1380)1/2^+$ state couples mostly to the $\pi^0\Lambda$ channel.

The resonances poles in the complex energy-plane are depicted and compared with the outcome of other models in Fig. 2. Note that all these models are purely s-wave approaches, and do not include the differential cross section data (b) that bears information on the partial-wave content. This is in line with the observation that, while there is a good agreement on the parameters of both poles in the s-wave with these models, the new p-wave state has not been found in any previous analyses.

Stability of results The predictions for the both poles of the $\Lambda(1405)1/2^-$ are well in agreement with other modern approaches [2, 11, 13]. The new p-wave $\Sigma(1380)1/2^+$-resonance has similar mass, width, and branching ratios as the decuplet $\Sigma(1385)3/2^+$ but different total angular momentum and is not listed in the PDG [35]. Before discussing the possible origin of this spurious state we perform several statistical and phenomenological tests to confirm its existence within the present model.

First: The $\pi\Sigma$-invariant mass distribution [53] from the reaction $K^-p\to\Sigma(1660)^+\pi^-\to((\pi\Sigma)\pi^+)\pi^-$ can be used for an *a-posteriori* test of the obtained solution. For this and following Ref. [18] we assume energy-independent production and decay vertices of the $\Sigma(1660)1/2^+$. Fitting the associated constants, while not altering the meson-baryon scattering amplitude in the final state, we obtain a good fit with $\chi^2_{\rm pp} = 0.89$. The result is shown in Fig. 6a in the Appendix.

Second: A similar test of our scattering amplitude can be performed using the $\pi\Sigma$-invariant mass distributions [54] of the reactions $\gamma p \to K^+(\pi\Sigma)$ recently measured with CLAS at Jefferson Lab. Following Refs. [2, 55] we obtain a good fit of the data with $\chi^2_{\rm pp} = 1.07$ (see Fig. 5 in the Appendix), fitting again only the generic couplings $\gamma N \to K^+\mathcal{S}_i$.

Third: The differential cross section data (b) contributes with 30% to the $\chi^2_{\rm dof}$, see Tab. I. Additionally, we test the impact of the these data by excluding it. Indeed, the generalized variance $|\Sigma|$ increases from $|\Sigma_{a,b,c} = 0.106$ to $|\Sigma_{a,c}| = 9.74$, i.e., the parameters of the model are significantly less well determined demonstrating the relevance of the differential cross sections. Furthermore, the $1(1/2^+)$ pole in the complex energy plane disappears – the existence of the $\Sigma(1380)1/2^+$ seems indeed tied to the differential cross section data.

Fourth: To investigate the stability of the new p-wave resonance further, we use the least absolute

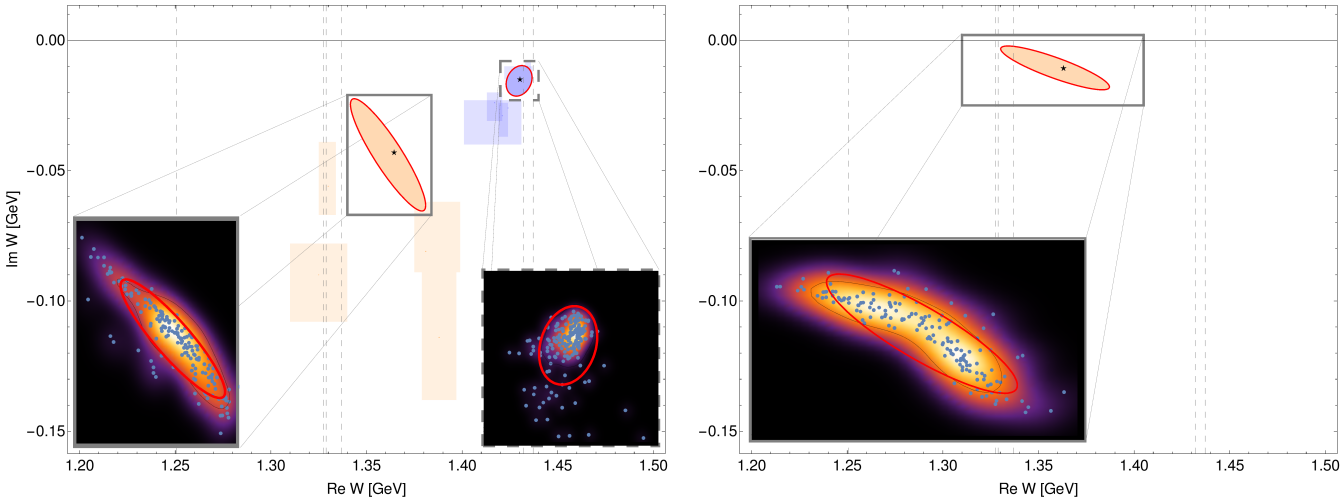

FIG. 2: Pole positions (black stars) for the $0(1/2^-)$ (left) and $1(1/2^+)$ (right) channels. The error ellipses are from a re-sampling procedure shown explicitly in the corresponding insets. The shaded squares show the prediction of Refs. [2, 11, 13] for the narrow (blue) and broad (orange) pole of $\Lambda(1405)$.

shrinkage and selection operator (LASSO) to remove the $\Sigma(1380)1/2^+$. In this we add a penalty term $\lambda \int_{1.29\,\mathrm{GeV}}^{1.46\,\mathrm{GeV}} |\partial^2/\partial W^2\, f_{1-}^{I=1}(W))| dW$ to the total χ^2. Minimizing this function at $\lambda = 0$ and including data (a,b,c) we obtain back our previous result. Subsequently increasing the value of λ and re-fitting, the curvature of the amplitude between the $\pi\Sigma$ and $\bar{K}N$ thresholds decreases forcing the p-wave resonance to disappear into the complex plane as shown in Fig. 6b. The figure also reveals that the description of the threshold data (c) deteriorates most visibly as the pole disappears. Of course, this is not *directly* due to the disappearance of the pole, but related to it through the low energy constants and logs.

We call the minimum λ at which the p-wave resonance is no longer visible on the amplitude at the real axis λ_{crit}. The difference in quality of the fit of the data when $\lambda = 0$ (our best fit) with the fit of the data at λ_{crit} measures the stability of the resonance. The likelihood ratio of the fit at $\lambda = \lambda_{\mathrm{crit}}$ to the fit at $\lambda = 0$ is 4.3×10^{-28} which shows that the data description indeed deteriorates significantly in the absence of the resonance. In particular, the prediction of kaonic hydrogen data [51] is more than 2 standard deviations away from the experimental value.

Interpretation As discussed in the previous section, the available experimental data require the presence of a new $1(1/2^+)$ resonance, analyzed in the present model. Notably, this model contains only s- and p-waves with $J = 1/2$, which explains the missing sub-threshold decuplet $\Sigma(1385)3/2^+$. In particular, the slope of the differential cross section indicates the size of the p-wave contribution (Fig. 4) but is blind to the total angular momentum. As a test, we have interchanged the amplitudes $f_{1-}^{I=1}$ and $f_{1+}^{I=1}$, effectively replacing the $\Sigma(1380)1/2^+$ by the decuplet $\Sigma(1385)3/2^+$. The description of the data, in particular the differential cross sections, barely changes. Furthermore, the $\Sigma(1380)1/2^+$ has not only a very similar pole position as the $\Sigma(1385)3/2^+$ but also very similar branching ratios into $\pi\Lambda$ and $\bar{K}N$ [35]. Thus, from a phenomenological point of view, the fit has generated the decuplet Σ, but with the wrong total angular momentum. Note also that no low-lying $1(1/2^+)$ state except for the ground-state Σ is found in lattice QCD calculations [28–30]. A possible way to clarify the role of p-wave resonances is to include the $\Sigma(1385)3/2^+$ as an explicit resonance state.

Conclusion For the first time the available low-energy differential cross section data have been included in a chiral unitary coupled-channel model with s- and p-waves. Parameters of both $\Lambda(1405)1/2^-$ poles are determined in this approach with improved stability. Additionally, and confirmed by multiple (statistical and phenomenological) tests, the data seem to require the existence of a p-wave pole but is otherwise insensitive to the total angular momentum. Thus, the p-wave pole is predicted in the only available p-wave with $J^P = 1/2^+$. Further understanding of this novel but spurious pole can be gained when explicitly including the p-wave decuplet $\Sigma(1385)3/2^+$ in the model or when data sensitive to the total angular momentum are available.

Acknowledgments MM thanks the German Research Association (MA 7156/1) for the financial support. MD acknowledges support by the National Science Foundation (grant nos. 1415459 and PHY-1452055) and by the U.S. Department of Energy, Office of Science, Office of Nuclear Physics under contract no. DE-AC05-06OR23177 and grant no. DE-SC0016582.

* dansadasivan@gwu.edu
† maximmai@gwu.edu
‡ doring@gwu.edu

[1] R. H. Dalitz and S. F. Tuan, Phys. Rev. Lett. **2**, 425 (1959).
[2] M. Mai and U.-G. Meißner, Eur. Phys. J. **A51**, 30 (2015), arXiv:1411.7884 [hep-ph].
[3] M. Mai and U.-G. Meissner, Nucl. Phys. **A900**, 51 (2013), arXiv:1202.2030 [nucl-th].
[4] A. Cieplý, M. Mai, U.-G. Meißner, and J. Smejkal, Nucl. Phys. **A954**, 17 (2016), arXiv:1603.02531 [hep-ph].
[5] K. Miyahara, T. Hyodo, and W. Weise, (2018), arXiv:1804.08269 [nucl-th].
[6] Z.-W. Liu, J. M. M. Hall, D. B. Leinweber, A. W. Thomas, and J.-J. Wu, Phys. Rev. **D95**, 014506 (2017), arXiv:1607.05856 [nucl-th].
[7] A. Ramos, A. Feijoo, and V. K. Magas, Nucl. Phys. **A954**, 58 (2016), arXiv:1605.03767 [nucl-th].
[8] Y. Kamiya, K. Miyahara, S. Ohnishi, Y. Ikeda, T. Hyodo, E. Oset, and W. Weise, Nucl. Phys. **A954**, 41 (2016), arXiv:1602.08852 [hep-ph].
[9] A. Feijoo, V. K. Magas, and A. Ramos, Phys. Rev. **C92**, 015206 (2015), arXiv:1502.07956 [nucl-th].
[10] R. Molina and M. Döring, Phys. Rev. **D94**, 056010 (2016), [Addendum: Phys. Rev.D94,no.7,079901(2016)], arXiv:1512.05831 [hep-lat].
[11] Z.-H. Guo and J. A. Oller, Phys. Rev. **C87**, 035202 (2013), arXiv:1210.3485 [hep-ph].
[12] M. Doring, J. Haidenbauer, U.-G. Meissner, and A. Rusetsky, Eur. Phys. J. **A47**, 163 (2011), arXiv:1108.0676 [hep-lat].
[13] Y. Ikeda, T. Hyodo, and W. Weise, Phys. Lett. **B706**, 63 (2011), arXiv:1109.3005 [nucl-th].
[14] A. Cieply and J. Smejkal, *Progress in strangeness nuclear physics. Proceedings, ECT Workshop on Strange Hadronic Matter, Trento, Italy, September 26-30, 2011*, Nucl. Phys. **A881**, 115 (2012), arXiv:1112.0917 [nucl-th].
[15] M. Doring, D. Jido, and E. Oset, Eur. Phys. J. **A45**, 319 (2010), arXiv:1002.3688 [nucl-th].
[16] J. A. Oller, Eur. Phys. J. **A28**, 63 (2006), arXiv:hep-ph/0603134 [hep-ph].
[17] E. Oset, A. Ramos, and C. Bennhold, Phys. Lett. **B527**, 99 (2002), [Erratum: Phys. Lett.B530,260(2002)], arXiv:nucl-th/0109006 [nucl-th].
[18] J. A. Oller and U.-G. Meißner, Phys. Lett. **B500**, 263 (2001), arXiv:hep-ph/0011146 [hep-ph].
[19] E. Oset and A. Ramos, Nucl. Phys. **A635**, 99 (1998), arXiv:nucl-th/9711022 [nucl-th].
[20] C. Fernandez-Ramirez, I. V. Danilkin, D. M. Manley, V. Mathieu, and A. P. Szczepaniak, Phys. Rev. **D93**, 034029 (2016), arXiv:1510.07065 [hep-ph].
[21] C. Fernandez-Ramirez, I. V. Danilkin, V. Mathieu, and A. P. Szczepaniak, Phys. Rev. **D93**, 074015 (2016), arXiv:1512.03136 [hep-ph].
[22] H. Kamano, S. X. Nakamura, T. S. H. Lee, and T. Sato, Phys. Rev. **C92**, 025205 (2015), [Erratum: Phys. Rev.C95,no.4,049903(2017)], arXiv:1506.01768 [nucl-th].
[23] H. Kamano, S. X. Nakamura, T. S. H. Lee, and T. Sato, Phys. Rev. **C90**, 065204 (2014), arXiv:1407.6839 [nucl-th].
[24] H. Zhang, J. Tulpan, M. Shrestha, and D. M. Manley, Phys. Rev. **C88**, 035205 (2013), arXiv:1305.4575 [hep-ph].
[25] H. Zhang, J. Tulpan, M. Shrestha, and D. M. Manley, Phys. Rev. **C88**, 035204 (2013), arXiv:1305.3598 [hep-ph].
[26] J. M. M. Hall, W. Kamleh, D. B. Leinweber, B. J. Menadue, B. J. Owen, and A. W. Thomas, Phys. Rev. **D95**, 054510 (2017), arXiv:1612.07477 [hep-lat].
[27] J. M. M. Hall, W. Kamleh, D. B. Leinweber, B. J. Menadue, B. J. Owen, A. W. Thomas, and R. D. Young, Phys. Rev. Lett. **114**, 132002 (2015), arXiv:1411.3402 [hep-lat].
[28] G. P. Engel, C. B. Lang, D. Mohler, and A. Schäfer (BGR), Phys. Rev. **D87**, 074504 (2013), arXiv:1301.4318 [hep-lat].
[29] R. G. Edwards, N. Mathur, D. G. Richards, and S. J. Wallace (Hadron Spectrum), Phys. Rev. **D87**, 054506 (2013), arXiv:1212.5236 [hep-ph].
[30] G. P. Engel, C. B. Lang, M. Limmer, D. Mohler, and A. Schafer (BGR [Bern-Graz-Regensburg]), Phys. Rev. **D82**, 034505 (2010), arXiv:1005.1748 [hep-lat].
[31] J.-J. Xie, J.-J. Wu, and B.-S. Zou, Phys. Rev. **C90**, 055204 (2014), arXiv:1407.7984 [nucl-th].
[32] C. Helminen and D. O. Riska, Nucl. Phys. **A699**, 624 (2002), arXiv:nucl-th/0011071 [nucl-th].
[33] R. L. Jaffe and F. Wilczek, Phys. Rev. Lett. **91**, 232003 (2003), arXiv:hep-ph/0307341 [hep-ph].
[34] F.-K. Guo, C. Hanhart, U.-G. Meißner, Q. Wang, Q. Zhao, and B.-S. Zou, Rev. Mod. Phys. **90**, 015004 (2018), arXiv:1705.00141 [hep-ph].
[35] C. Patrignani *et al.* (Particle Data Group), Chin. Phys. **C40**, 100001 (2016).
[36] M. Agnello *et al.* (FINUDA), Phys. Rev. Lett. **94**, 212303 (2005).
[37] D. B. Kaplan and A. E. Nelson, Phys. Lett. **B175**, 57 (1986).
[38] S. Pal, D. Bandyopadhyay, and W. Greiner, Nucl. Phys. **A674**, 553 (2000), arXiv:astro-ph/0001039 [astro-ph].
[39] J. Abadie *et al.* (LIGO Scientific), Nature Phys. **7**, 962 (2011), arXiv:1109.2295 [quant-ph].
[40] M. Mai, *From meson-baryon scattering to meson photoproduction*, Ph.D. thesis, Bonn U., HISKP (2013).
[41] J. Gasser and H. Leutwyler, Nucl. Phys. **B250**, 465 (1985).
[42] P. C. Bruns, M. Mai, and U. G. Meissner, Phys. Lett. **B697**, 254 (2011), arXiv:1012.2233 [nucl-th].
[43] G. Hohler, *NUMERICAL DATA AND FUNCTIONAL RELATIONSHIPS* , edited by H. Schopper (1984).
[44] J. Ciborowski *et al.*, J. Phys. **G8**, 13 (1982).
[45] W. E. Humphrey and R. R. Ross, Phys. Rev. **127**, 1305 (1962).
[46] M. Sakitt, T. B. Day, R. G. Glasser, N. Seeman, J. H. Friedman, W. E. Humphrey, and R. R. Ross, Phys. Rev. **139**, B719 (1965).
[47] M. B. Watson, M. Ferro-Luzzi, and R. D. Tripp, Phys. Rev. **131**, 2248 (1963).
[48] T. S. Mast, M. Alston-Garnjost, R. O. Bangerter, A. S. Barbaro-Galtieri, F. T. Solmitz, and R. D. Tripp, Phys. Rev. **D14**, 13 (1976).
[49] D. N. Tovee *et al.*, Nucl. Phys. **B33**, 493 (1971).
[50] R. J. Nowak *et al.*, Nucl. Phys. **B139**, 61 (1978).
[51] M. Bazzi *et al.* (SIDDHARTA), Phys. Lett. **B704**, 113 (2011), arXiv:1105.3090 [nucl-ex].

[52] U. G. Meissner, U. Raha, and A. Rusetsky, Eur. Phys. J. **C35**, 349 (2004), arXiv:hep-ph/0402261 [hep-ph].
[53] R. J. Hemingway, Nucl. Phys. **B253**, 742 (1985).
[54] K. Moriya *et al.* (CLAS), Phys. Rev. **C87**, 035206 (2013), arXiv:1301.5000 [nucl-ex].
[55] L. Roca and E. Oset, Phys. Rev. **C87**, 055201 (2013), arXiv:1301.5741 [nucl-th].

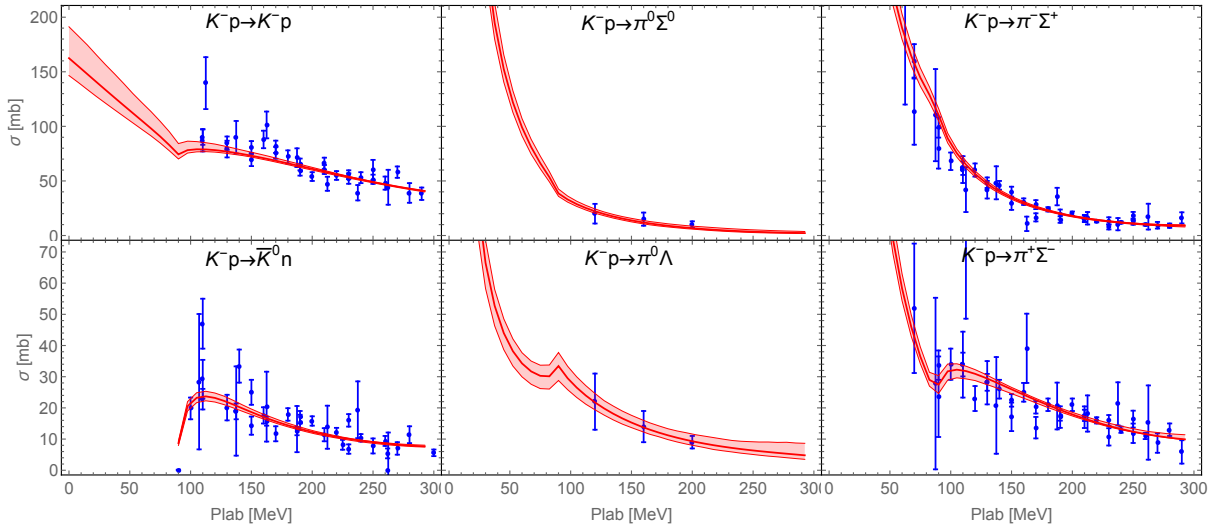

FIG. 3: Total cross sections [44, 45, 47, 50] fitted by the model described in the main part of the manuscript. Error bands represent the 1σ uncertainty determined in a re-sampling procedure.

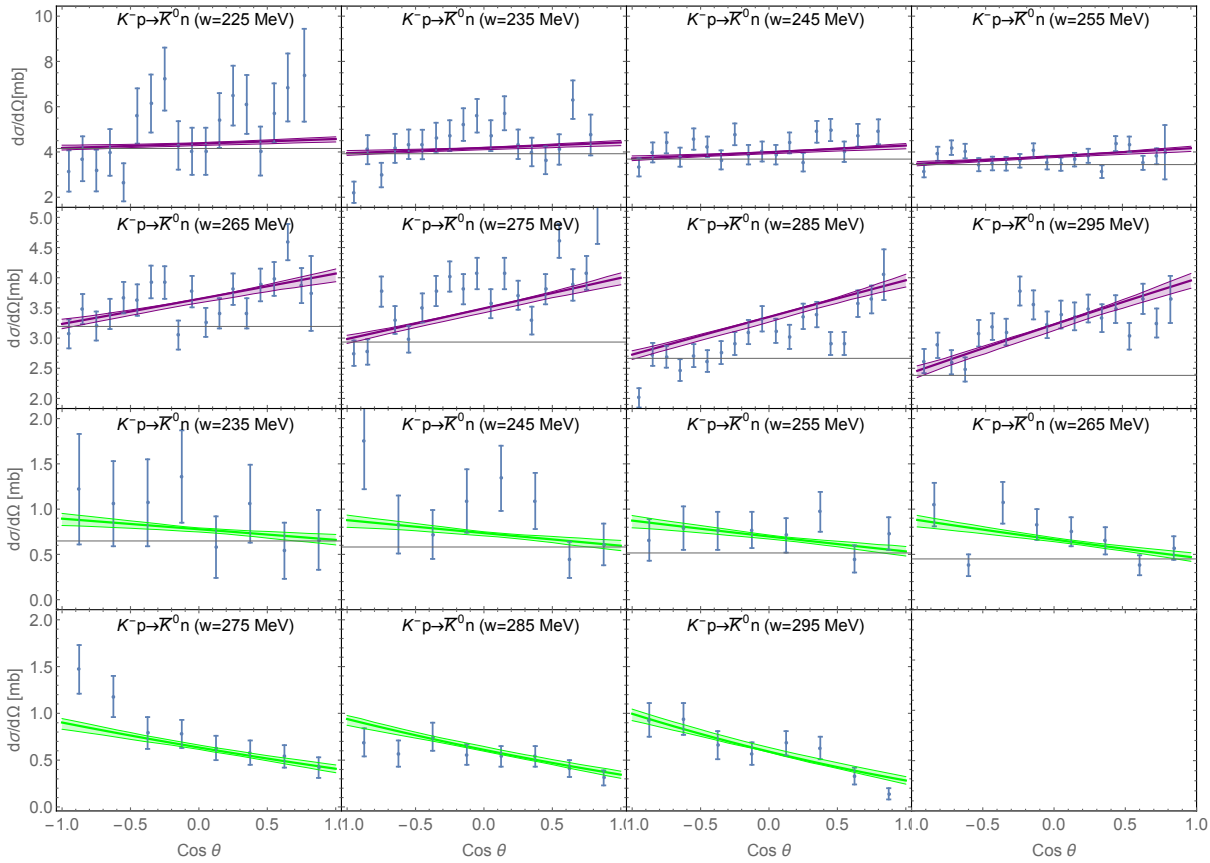

FIG. 4: Differential cross sections [48] fitted by the model described in the main part of the manuscript. Error bands represent 1σ uncertainty determined in a re-sampling procedure.

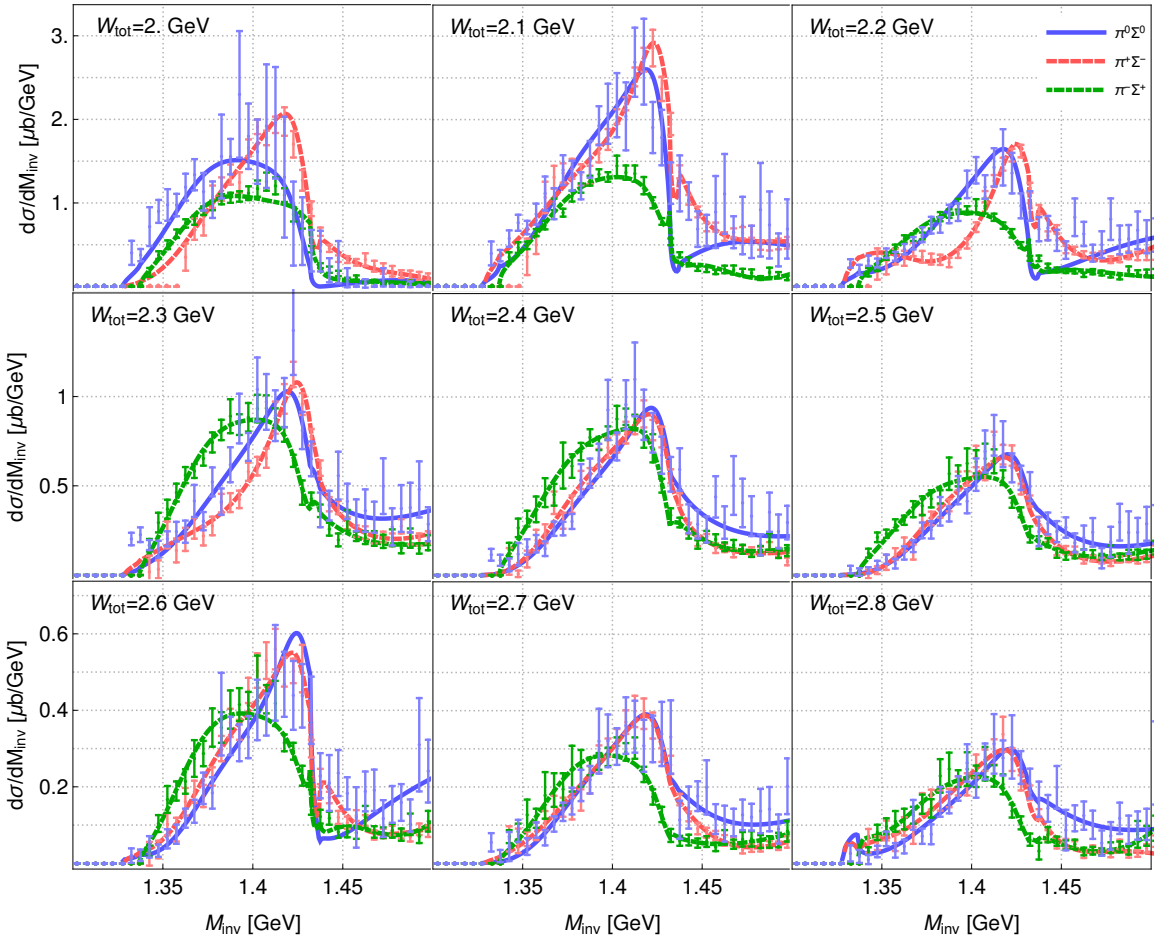

FIG. 5: Fit ($\chi^2_{\rm pp} = 1.07$) to the $\pi\Sigma$ invariant mass distribution from $\gamma p \to K^+(\pi\Sigma)$ reaction [54]. The model for the reaction is taken from Ref. [2], where only generic couplings $\gamma p \to K^+\mathcal{S}$ are fitted to the data. The meson-baryon scattering amplitude in the final state is taken from the fit to the scattering data. Error bands are ignored in this a-posteriori compatibility test.

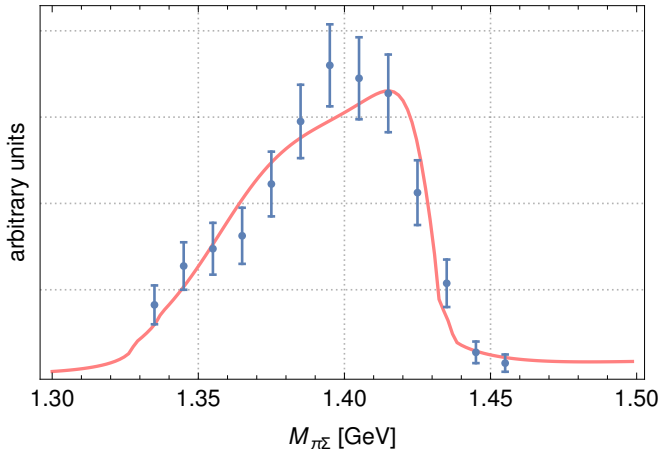

(6a) Fit of the generic couplings $K^-p \to \Sigma(1660)\pi^-$, $\Sigma(1660) \to (\pi\Sigma)\pi^+$ to the invariant mass distribution [53] in arbitrary units. The final state interaction is taken from the best fit to the scattering data as described in the main part of the manuscript. Only the best fit is shown.

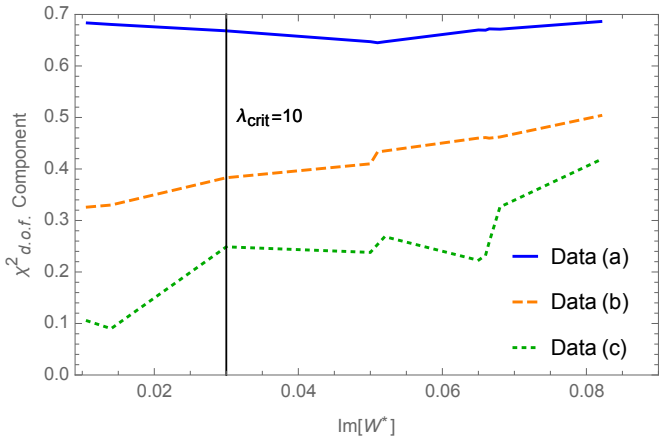

(6b) Dependence of the components of the $\chi^2_{\rm dof}$ from each data set on the distance of the W^* pole from the real axis, parametrized with the penalty λ. The sum of all three components equals $\chi^2_{d.o.f.}$ which increases with the imaginary position of the pole at $W = W^*$. The contribution to the χ^2 from the penalty is subtracted in all cases.